Petrology, Geochemistry (Geochronology)

The Montalet granite, Montagne Noire, France: An Early Permian syn-extensional pluton as evidenced by new U-Th-Pb data on zircon and monazite

Le granite du Montalet, Montagne Noire, France : un pluton syn-extension du Permien inférieur, mis en évidence par la datation U-Th-Pb sur zircons et monazites

Jean-Charles Poilvet [a], Marc Poujol [a,*], Pavel Pitra [a], Jean Van Den Driessche [a], Jean-Louis Paquette [b]

[a] Université Rennes 1, Géosciences Rennes, UMR CNRS 6118, 35042 Rennes cedex, France
[b] Université Blaise-Pascal, Laboratoire Magmas et Volcans, UMR CNRS 6524, 63038 Clermont-Ferrand cedex, France

ARTICLE INFO

ABSTRACT

Dating the magmatism in the Montagne Noire gneiss dome in the southern French Massif Central is a key point for understanding the Late Palaeozoic evolution of this part of the Variscan belt, which is characterised by compressive tectonics during the Carboniferous and extensional tectonics during Stephanian-Permian times. The Montalet granite crops out in the north-western part of the dome and was first considered as an early syntectonic intrusion related to compressive deformation. More recently, it has been dated at 327 Ma and considered as contemporaneous with the diapiric ascent of the Montagne Noire gneiss dome before the Stephanian-Permian extension. We show that in fact, this pluton was emplaced 294 ± 1 Ma ago and is therefore contemporaneous with the Stephanian-Permian extension. This age is consistent with the interpretation of the Montagne Noire Massif as an extensional gneiss dome.

© 2011 Académie des sciences. Published by Elsevier Masson SAS. All rights reserved.

RÉSUMÉ

La datation du magmatisme dans le dôme gneissique de la Montagne Noire est un point-clé pour la compréhension de l'évolution de cette partie de la chaîne varisque pendant le Paléozoïque supérieur, laquelle est caractérisée par une tectonique compressive pendant le Carbonifère, puis par une tectonique extensive pendant le Stéphano-Permien. Le granite du Montalet qui affleure dans la partie nord-ouest du dôme a d'abord été considéré comme une intrusion syntectonique reliée à une tectonique compressive précoce. Il a été daté à 327 Ma et considéré comme contemporain de l'ascension diapirique du dôme, avant l'extension stéphano-permienne. Nous montrons qu'en fait ce granite se met en place à 294 Ma et est donc contemporain de l'extension stéphano-permienne. Cet âge est cohérent avec l'interprétation de la Montagne Noire comme un dôme gneissique extensif.

© 2011 Académie des sciences. Publié par Elsevier Masson SAS. Tous droits réservés.

* Corresponding author.
 *E-mail address:* marc.poujol@univ-rennes1.fr (M. Poujol).

1. Introduction

The timing and tectonic settings of the Late Paleozoic uplift of the Montagne Noire gneiss dome in the southern French Massif Central (MC) are still the subject of controversy. Three main tectonic interpretations have been proposed so far (Charles et al., 2009; Van Den Driessche and Brun, 1992 and references therein): diapiric ascent, compression resulting in a regional anticline, and extension resulting in a core complex. The two first interpretations consider that the dome rose during the Late Carboniferous compression before the regional Permian extensional tectonics. In the third interpretation, the extension started as early as the Late Carboniferous, resulting in the dome uplift, and continued during the Permian. Synmetamorphic ductile deformation that accompanied the dome uplift is attributed to diapirism or compression for the first and second interpretations, respectively, whereas it resulted from deep-seated extension that overprinted previous compression in the third interpretation. Magmatism is attributed to partial crustal melting consecutive to crustal thickening in the three models, but deformation of the plutons, when present, is interpreted in accordance with each of the mechanisms proposed for the dome uplift.

The age of the plutons is therefore a key datum that can help to discriminate between these different models. The Montalet granite is one of these plutons, with a deformation history that is still controversial (Brun and Van Den Driessche, 1996; Demange, 1996).

According to Demange et al. (1995) "the precise dating of this granite would undoubtedly solve many problems of the regional geology on the Montagne Noire".
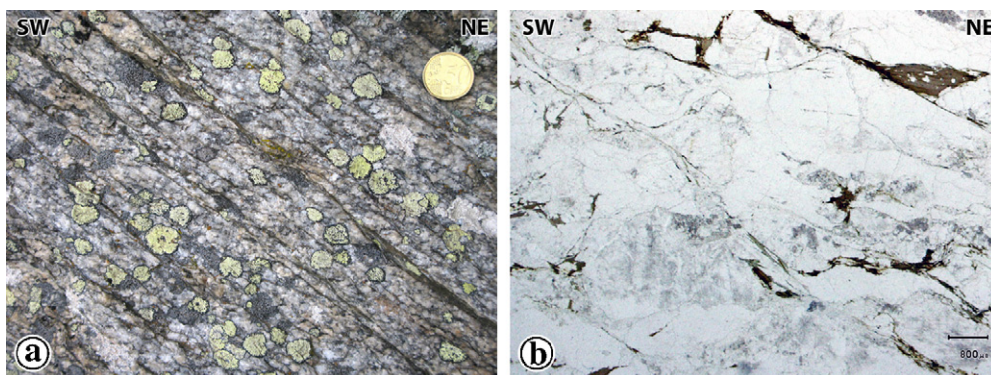
2. The Montalet granite

The Montalet granite crops out along the northwestern edge of the Montagne Noire gneiss dome (Fig. 1). The granite is composed of sills or laccoliths ranging in thickness from a few tens of metres to several hundreds metres (Demange et al., 1995). The deformation of the granite increases toward the major tectonic contact that limits the gneiss dome to the north and northwest. This contact is referred to as the Lacaune fault (Demange, 1996) or the Espinouse detachment (Brun and Van Den Driessche, 1994), respectively. According to Demange (1996), a magmatic foliation developed first and was then crosscut by a second foliation when approaching the Lacaune fault, as both planar structures are related to early thrusting events. For Brun and Van Den Driessche (1996), these two planar structures correspond to S-C structures (Berthé et al., 1979) (Fig. 2a) that developed during a single extensional shearing deformation along the Espinouse detachment. But in both cases, these authors consider that the Montalet granite is syn-kinematic in nature. We chose to sample this granite at the Col de Picotalen (or Piquotalen) (Fig. 2a), the location that these two conflicting interpretations are based upon, as it shows a well-developed deformation, (43° 41′ 16. 53″ N, 2° 39′ 33. 38″E).
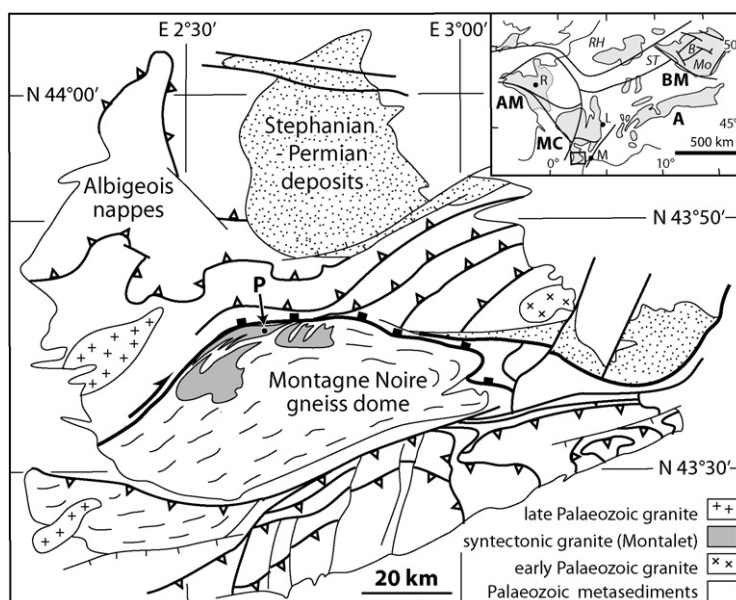
Fig. 1. Structural map of the southern French Massif Central (MC) showing the relationships between the Montagne Noire gneiss dome, the Stephanian-Permian basins, and the Variscan thrusts and nappes. P.: Col of Picotalen (sampling site). Inset shows the location of the study area within the European Variscan belt (modified from Pitra et al., 2010). A: Alps; AM: Armorican Massif; BM: Bohemian Massif; MC: Massif Central. B: Teplá-Barrandian; Mo: Moldanubian; ST: Saxothuringian; RH: Rhenohercynian. L: Lyon; M: Montpellier; R: Rennes.

Fig. 1. Schéma structural du Sud du Massif Central (MC) montrant les relations entre le dôme gneissique de la Montagne Noire, les bassins stéphano-permiens et les nappes et chevauchements varisques. P. : Col de Picotalen (site d'échantillonnage). L'encart montre la position de la zone d'étude dans la chaîne varisque européenne (modifié d'après Pitra et al., 2010). A : Alpes ; AM : Massif Armoricain ; BM : Massif de Bohême ; MC : Massif Central ; B : Teplá-Barrandien ; Mo : Moldanubien ; ST : Saxothuringien ; RH : Rhénohercynien. L : Lyon ; M : Montpellier ; R : Rennes.

Fig. 2. The Montalet granite. **a**: Outcrop of the Montalet granite at the Col de Picotalen. Orientation SW-NE.; **b**: Microscopic aspect in plane polarised light (thin section parallel to the $\lambda_1\lambda_3$ plane of deformation). Orientation SW-NE. Feldspar crystals, quartz ribbons and a large biotite crystal define the foliation S. Discrete NE-dipping planes marked by fine grained crystals including chlorite are the C-planes.

Fig. 2. Le granite du Montalet. **a** : affleurement du granite du Montalet au col de Picotalen. Orientation SW-NE ; **b** : aspect en microscopie en lumière polarisée non analysée (lame mince parallèle au plan de déformation $\lambda_1\lambda_3$). Orientation SW-NE. Les cristaux de feldspath, les rubans de quartz et le grand cristal de biotite définissent la foliation S. Les plans discrets soulignés par des cristaux de petite taille, dont la chlorite, sont les plans C.

The Montalet granite is a garnet-bearing, two-mica leucogranite. The selected sample is composed of K-feldspar, plagioclase, quartz, biotite, muscovite, garnet and accessory minerals. The main foliation S is marked by the shape preferred orientation of feldspar porphyroclasts (up to 10 mm long), micas (up to 3 mm) and quartz aggregates (Fig. 2b). Subhedral K-feldspar generally lacks strong internal deformation and displays Carlsbad twin planes, generally parallel to the foliation S. The feldspars include quartz droplets and biotite and muscovite crystals inherited from the early magmatic stage. Very small (0.01–0.03 mm) grains of quartz and micas are contained within regular narrow bands, spaced by 5 to 10 mm in general, interpreted as shear bands C (Figs. 2a and b). In the vicinity of these shear bands, biotite and garnet are locally replaced by chlorite. Quartz ribbons affected by these shear bands display progressive reorientation and grain size reduction towards the shear band. The foliation strikes east-west and dips ca. 20° to the north. The stretching lineation L underlined by the long axis of quartz, micas and feldspar clasts plunges about 15° NE. The C-planes dip ca. 50° to the north, some 20 to 30° steeper than the foliation, indicating a deformation associated with a normal movement to the northeast. They bear fine striae plunging about 45° to the northeast.

The preferred orientation of the subhedral feldspar crystals may be attributed to deformation affecting a partly crystallised magma. Pervasive S-C type structures suggest intense, solid state deformation. Myrmekites that developed at the K-feldspar high-pressure sides suggest diffusion and consequently high-temperature deformation (Simpson and Wintsch, 1989). Quartz constitutes polycrystalline ribbons parallel to the foliation. Recrystallised grains are slightly elongated, forming an internal shape fabric oblique to S. Lobate boundaries suggest some recrystallisation by grain boundary migration, common at high temperatures (e.g. Gapais and Barbarin, 1986). Biotite crystals have typical fish-like shapes and tend to be replaced by chlorite, which is interpreted as a consequence of cooling. The grain size evolution from the foliation to the shear bands also suggests progressive deformation at decreasing temperature.

The S-C structures indicate a top to the northeast shear as supported by internal quartz schistosity and mica fishes. This means that the Montalet granite was deformed syntectonically during its emplacement into the footwall of a normal, ductile shear zone.

3. Dating

3.1. Analytical techniques

A classic mineral separation procedure has been applied to concentrate minerals suitable for U-Th-Pb dating using the facilities available at Géosciences Rennes. Rocks were crushed and only the powder fraction with a diameter < 250 μm has been kept. Heavy minerals were successively concentrated by Wilfley table and heavy liquids. Magnetic minerals were then removed with an isodynamic Frantz separator. Zircon and monazite grains were carefully handpicked under a binocular microscope and embedded in epoxy mounts. The grains were then hand-grounded and polished on a lap wheel with a 6 μm and 1 μm diamond suspension successively. Zircons were imaged by cathodoluminescence (CL) using a Reliotron CL system equipped with a digital color camera available in Géosciences Rennes.

U-Th-Pb geochronology of zircon and monazite was conducted by in situ laser ablation inductively coupled plasma mass spectrometry (LA-ICPMS) at the Laboratoire Magmas et Volcans in Clermont-Ferrand, France. Ablation spot diameters of 26 μm and 7 μm with repetition rates of 3 Hz and 1 Hz were used for zircon and monazite, respectively. Data were corrected for U-Pb and Th-Pb fractionation and for the mass bias by standard bracketing with repeated measurements of the 91,500 zircon (Wiedenbeck et al., 1995) or the Moacir monazite standards (Gasquet et al., 2010). Repeated analyses of GJ-1 zircon (Jackson et al., 2004) or Manangoutry monazite (Paquette and Tiepolo, 2007) standards treated as unknowns were used to control the reproducibility and

Table 1
LA-ICP-MS U-Th-Pb data for monazite and zircon from sample ES5. Uncertainties are given at the one sigma level.

Tableau 1
Données U-Th-Pb obtenues par LA-ICP-MS sur des zircons et monazites de l'échantillon ES5. Les erreurs sont données à 1 sigma.

Analysis	[Pb] ppm	[U] ppm	[Th] ppm	^{207}Pb/^{235}U	Err	^{206}Pb/^{238}U	Err	rho	^{208}Pb/^{232}Th	Err	AGES ^{207}Pb/^{206}Pb	Err	^{206}Pb/^{238}U	Err	^{207}Pb/^{235}U	Err	^{208}Pb/^{232}Th	Err
ES5 Monazites																		
07120410a	1177	2673	82,272	0.326	0.006	0.0464	0.0006	0.67	0.0144	0.0002	238	42	292	4	286	5	289	3
08120410a	977	2580	66,302	0.388	0.007	0.0473	0.0006	0.70	0.0145	0.0002	586	38	298	4	333	5	292	3
09120410a	819	4245	50,155	0.330	0.005	0.0471	0.0006	0.76	0.0144	0.0002	233	36	297	4	289	4	289	3
10120410a	880	2289	59,156	0.323	0.006	0.0468	0.0006	0.67	0.0147	0.0002	199	43	295	4	284	5	295	3
11120410a	1081	3598	71,034	0.329	0.006	0.0467	0.0006	0.75	0.0146	0.0002	243	37	294	4	289	4	293	3
12120410a	1035	5368	61,578	0.331	0.005	0.0469	0.0006	0.79	0.0148	0.0002	249	33	296	4	291	4	298	3
13120410a	913	1500	63,069	0.332	0.007	0.0482	0.0006	0.60	0.0148	0.0002	197	49	303	4	291	6	298	3
14120410a	1019	1370	72,100	0.344	0.008	0.0483	0.0006	0.58	0.0147	0.0002	269	51	304	4	300	6	294	3
18120410a	1135	3982	74,153	0.329	0.006	0.0461	0.0006	0.75	0.0146	0.0002	280	36	290	4	289	4	292	3
19120410a	856	1566	59,623	0.340	0.008	0.0477	0.0006	0.59	0.0146	0.0002	273	50	300	4	297	6	293	3
20120410a	1011	2339	69,365	0.516	0.009	0.0485	0.0006	0.75	0.0144	0.0002	1125	32	305	4	422	6	290	3
21120410a	1093	6883	63,307	0.328	0.005	0.0464	0.0006	0.81	0.0144	0.0002	251	32	293	4	288	4	290	3
22120410a	1074	2562	72,339	0.333	0.006	0.0474	0.0006	0.68	0.0147	0.0002	239	41	298	4	292	5	295	3
23120410a	915	6262	52,282	0.322	0.005	0.0463	0.0006	0.80	0.0143	0.0002	214	33	292	4	283	4	286	3
24120410a	998	5730	59,651	0.368	0.006	0.0465	0.0006	0.81	0.0143	0.0002	508	31	293	4	318	4	287	3
28120410a	1272	2248	89,612	0.329	0.007	0.0467	0.0006	0.63	0.0144	0.0002	249	45	294	4	289	5	289	3
29120410a	849	6263	46,830	0.323	0.005	0.0462	0.0006	0.79	0.0143	0.0002	228	33	291	4	284	4	288	3
30120410a	1200	3034	80,608	0.336	0.006	0.0472	0.0006	0.70	0.0146	0.0002	270	39	297	4	294	5	293	3
31120410a	1052	3031	70,357	0.331	0.006	0.0470	0.0006	0.68	0.0145	0.0002	245	41	296	4	290	5	291	3
32120410a	1210	4462	76,896	0.326	0.005	0.0470	0.0006	0.75	0.0147	0.0002	213	37	296	4	287	4	295	3
33120410a	1199	2604	81,655	0.331	0.006	0.0466	0.0006	0.68	0.0146	0.0002	268	41	294	4	291	5	294	3
34120410a	1028	1808	72,787	0.329	0.008	0.0463	0.0006	0.54	0.0143	0.0002	261	56	292	4	288	6	287	3
35120410a	879	3079	56,592	0.322	0.006	0.0470	0.0006	0.68	0.0146	0.0002	179	41	296	4	283	5	293	3
38120410a	951	2748	63,216	0.342	0.007	0.0471	0.0006	0.67	0.0145	0.0002	314	42	297	4	299	5	291	3
39120410a	1053	3077	69,110	0.326	0.006	0.0467	0.0006	0.69	0.0147	0.0002	228	40	294	4	287	5	295	3
40120410a	1320	4158	86,214	0.331	0.006	0.0473	0.0006	0.72	0.0146	0.0002	228	38	298	4	290	4	293	3
41120410a	999	1602	69,532	0.338	0.008	0.0473	0.0006	0.59	0.0146	0.0002	277	50	298	4	296	6	293	3
43120410a	1186	2065	81,776	0.337	0.007	0.0475	0.0006	0.61	0.0146	0.0002	264	47	299	4	295	5	294	3

Table 1 (*Continued*)

Analysis	[Pb] ppm	[U] ppm	[Th] ppm	$^{207}Pb/^{235}U$	Err	$^{206}Pb/^{238}U$	Err	rho	$^{208}Pb/^{232}Th$	Err	AGES $^{207}Pb/^{206}Pb$	Err	$^{206}Pb/^{238}U$	Err	$^{207}Pb/^{235}U$	Err	$^{208}Pb/^{232}Th$	Err
44120410a	1224	3685	80,665	0.327	0.006	0.0465	0.0006	0.69	0.0146	0.0002	245	40	293	4	288	5	292	3
45120410a	1212	2394	83,074	0.334	0.007	0.0471	0.0006	0.62	0.0146	0.0002	260	46	297	4	293	5	293	3

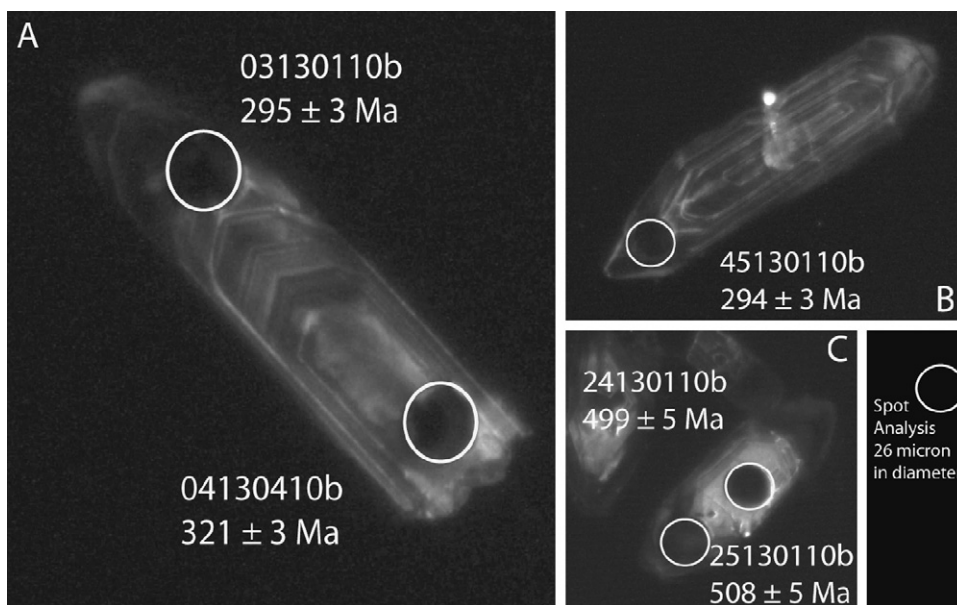|	[Pb] ppm	[U] ppm	$^{207}Pb/^{235}U$	Err	$^{206}Pb/^{238}U$	Err	rho	$^{207}Pb/^{206}Pb$	Err	AGES $^{207}Pb/^{206}Pb$	Err	$^{206}Pb/^{238}U$	Err	$^{207}Pb/^{235}U$	Err
ES5 Zircons															
03130410b	59	1525	0.337	0.004	0.0454	0.0005	0.93	0.0538	0.0006	363	26	286	3	295	3
04130410b	42	1019	0.372	0.005	0.0514	0.0006	0.92	0.0524	0.0006	304	26	323	4	321	3
05130410b	43	1026	0.375	0.005	0.0513	0.0006	0.92	0.0530	0.0006	330	25	323	4	324	3
10130410b	19	507	0.352	0.005	0.0451	0.0005	0.87	0.0565	0.0007	472	27	284	3	306	3
13130410b	35	935	0.354	0.004	0.0448	0.0005	0.92	0.0573	0.0007	503	25	282	3	308	3
17130410b	75	2042	0.335	0.004	0.0464	0.0005	0.95	0.0524	0.0006	304	25	292	3	294	3
18130410b	57	1438	0.336	0.004	0.0465	0.0005	0.93	0.0525	0.0006	307	26	293	3	294	3
24130410b	44	688	0.635	0.008	0.0796	0.0009	0.90	0.0579	0.0007	525	26	494	5	499	5
25130410b	51	812	0.650	0.008	0.0788	0.0009	0.91	0.0598	0.0007	597	25	489	5	508	5
26130410b	43	1057	0.341	0.004	0.0472	0.0005	0.89	0.0524	0.0006	301	26	297	3	298	3
30130410b	32	794	0.332	0.005	0.0453	0.0005	0.83	0.0531	0.0007	334	29	286	3	291	3
34130410b	122	3233	0.334	0.004	0.0466	0.0005	0.90	0.0520	0.0006	286	27	294	3	293	3
35130410b	17	352	0.423	0.006	0.0565	0.0007	0.79	0.0543	0.0008	383	31	354	4	358	4
37130410b	44	1121	0.341	0.004	0.0468	0.0005	0.90	0.0529	0.0006	323	27	295	3	298	3
38130410b	23	589	0.337	0.005	0.0458	0.0005	0.81	0.0533	0.0007	342	31	289	3	295	4
39130410b	93	2511	0.340	0.004	0.0462	0.0005	0.88	0.0533	0.0007	342	27	291	3	297	3
40130410b	53	1428	0.343	0.004	0.0446	0.0005	0.88	0.0557	0.0007	441	26	281	3	299	3
44130410b	148	4044	0.337	0.005	0.0443	0.0005	0.84	0.0552	0.0007	422	28	279	3	295	3
45130410b	50	1248	0.336	0.004	0.0467	0.0005	0.89	0.0521	0.0006	291	27	294	3	294	3
46130410b	22	587	0.341	0.005	0.0439	0.0005	0.83			465	29	277	3	298	4
48130410b	48	1284	0.342	0.004	0.0446	0.0005	0.88			438	27	281	3	299	3
50130410b	11	245	0.397	0.007	0.0516	0.0006	0.70			443	36	324	4	339	5

Fig. 3. Cathodoluminescence images of some of the zircon grains dated in this study.

Fig. 3. Photos en cathodoluminescence de certains des zircons datés lors de cette étude.

accuracy of the corrections. Data reduction was carried out with the GLITTER® software package developed by the Macquarie Research Ltd. (Jackson et al., 2004). Concordia ages and diagrams were generated using Isoplot/Ex (Ludwig, 2001). All errors given in Table 1 are listed at one sigma, but where data are combined for regression analysis or to calculate weighted means, the final results are provided with 95% confidence limits. Further information on the instrumentation and the analytical technique is detailed in Hurai et al. (2010).

3.2. Results

Monazite grains were generally euhedral and yellowish. Thirty grains were analysed and the data are reported in Table 1. In a $^{206}Pb/^{238}U$ versus $^{208}Pb/^{232}Th$ diagram, they all plot in a concordant to sub-concordant position (Fig. 4a) and define a Concordia age (Ludwig, 1998) of 293.66 ± 0.96 Ma (MSWD = 18), which is within the error with the mean average $^{208}Pb/^{232}Th$ date of 291.9 ± 3.3 Ma (MSWD = 0.89).
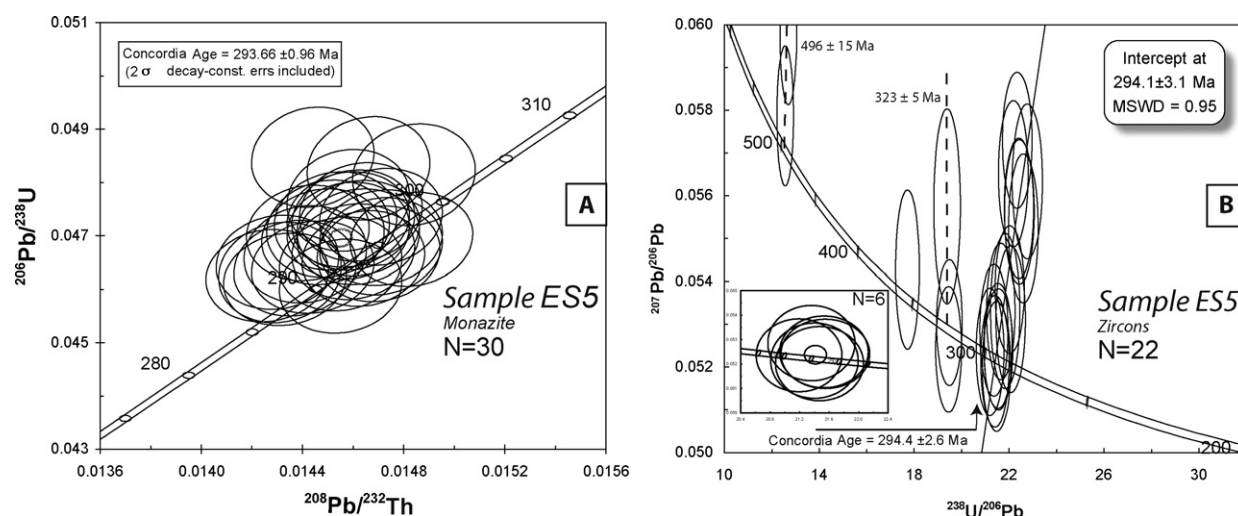

Fig. 4. $^{206}Pb/^{238}U$ versus $^{208}Pb/^{232}Th$ Concordia diagram for monazites (A) and Terra Wasserburg diagram (B) for zircons from sample ES5. All ellipses are represented at 1 sigma level. All ages are quoted at 2 sigma level.

Fig. 4. Diagramme Concordia $^{206}Pb/^{238}U$ versus $^{208}Pb/^{232}Th$ pour les monazites (A) et diagramme Terra Wasserburg pour les zircons (B) de l'échantillon ES5. Toutes les ellipses d'erreurs sont représentées à un sigma. Tous les âges sont donnés à deux sigmas.

Zircons were translucent to pinkish, euhedral and generally elongated. Cathodoluminescence imaging of the grains revealed a bright core with magmatic zoning surrounded by darker rims (Fig. 3). Twenty-two analyses were performed on twenty grains (Table 1). During the course of the analyses, several zircons showed the presence of common Pb, but no correction was applied. Plotted in a Terra Wasserburg diagram (Fig. 4b), the data do not define a simple trend with apparent dates ranging from ca. 500 Ma down to 295 Ma. A first group with two analyses (24130410b and 25130410b) defines a date around 496 ± 15 Ma. A second group with three analyses (04130410b, 05130410b and 50130410b) defines a date of 323 ± 5 Ma. The last group defined by six concordant analyses allows one to calculate a Concordia age of 294.4 ± 2.6 Ma (MSWD = 0.51; Fig. 4b, insert). The remaining points plot in a sub-concordant to discordant position. We believe that their position can be linked to the combined effect of the presence of "common" Pb incorporated in some of the grains and a slight Pb loss. The presence of initial "common" Pb in some of the grains is attested by the fact that several zircon grains present a slight (few tens of counts) positive ^{204}Pb value. This common Pb might have been present in some small inclusions not detected during imaging or related to fractures or areas of radiation damage. In the Terra Wasserburg diagram (Fig. 4b), these data, together with the previous six concordant allow a discordia to be drawn with a lower intercept of 293.7 ± 2.3 (MSWD = 0.88). In light of the present data, which are all consistent within error regardless of whether common Pb was detected or not, we thus conclude that zircon crystallisation took place 294 ± 3 Ma ago. In this scenario, the remaining older ages must be attributed to inheritance. This age of 294 ± 3 Ma is also identical to the age of 294 ± 1 Ma found for the monazites. Consequently, we conclude that the Montalet granite was emplaced during the Early Permian, ca. 294 Ma ago.

4. Discussion – conclusion

Petrological and structural data show that the Montalet granite is a syntectonic intrusion that cooled progressively during a continuous deformation from magmatic to solid states. The 294 ± 1 Ma age of the Montalet granite demonstrates that it was emplaced during the Late Paleozoic extension in the ductile lower crust, contemporaneously with the: (1) ductile shearing event related to the Espinouse detachment and; (2) sedimentation within the Stephanian-Permian Graissessac-Lodève basin.

Indeed, similar ^{40}Ar/^{39}Ar ages of 297 ± 3 Ma have been obtained by Maluski et al. (1991) on biotite and muscovite from sheared orthogneisses, in the footwall of the Espinouse detachment, and were also interpreted as S-C mylonites (Beaud, 1985; Burg et al., 1994; Echtler and Malavieille, 1990; Van Den Driessche and Brun, 1992). Bruguier et al. (2003) published an age of 295 ± 5 Ma for zircons extracted from a volcanic ash layer interbedded in the Late Carboniferous sedimentary fill of the Graissessac-Lodève basin, developed in the hangingwall of the Espinouse detachment (Fig. 1). Similar ages, ranging from 295 to 300 Ma have also been reported by the same authors in other Late Carboniferous extensional basins of the southern French MC, demonstrating an intense magmatic activity during this period (Bruguier et al., 2003).

On the other hand, Bé Mézème (2005) and Faure et al. (2010) have analysed monazites and zircons from the same pluton, but which was sampled in three sites located several kilometres farther to the south-west (Fig. 1).

Zircons were dated at 324 ± 3 Ma by SIMS and monazites at 327 ± 7 Ma by EPMA. At this stage, it has to be noted that four concordant to sub-concordant zircons analysed by Faure et al. (2010) plot in a "younger" position than the nine grains used to calculate the age of 324 ± 3 Ma (Figure 12C of Faure et al., 2010). A mixing discordia between common Pb and radiogenic Pb for these four "younger" points yields a date of 305 ± 29 Ma (MSWD = 0.78). The significance of these four points has not been discussed in the paper. However, it is interesting to note that this date of ca. 305 Ma is within the error of the age of 294 ± 3 Ma found for the zircons in this study. Furthermore, we also demonstrate the existence of inherited cores within our zircon population that are dated at ca. 323 Ma.

As for the monazites, Faure et al. (2010) analysed three different samples of the Montalet granite. Two of them yielded EPMA ages of 333 ± 4 Ma and 327 ± 7 Ma, respectively. For this second sample, it is interesting to note the discrepancy between the U-Pb age (289 +43/–49 Ma) and the Th-Pb age (349 +28/–25 Ma) and the fact that the theoretical isochron is barely within the error envelope. The last sample yielded an EPMA age of 499 ± 6 Ma. This indubitably shows the presence of inherited monazites within at least one of their samples (which they acknowledge on page 665). Because of the intrinsic principles of the EPMA technique, one cannot therefore exclude the presence of inherited Pb (^{208}Pb?) within some of the monazites from the remaining two samples, which would have resulted in a meaningless older age.

Another explanation to account for the difference between the ages published by Faure et al. (2010) and the ages found in this study could be that we dated two different intrusions corresponding to two magmatic pulses that are separated in time, yet mapped as a single intrusion known as the Montalet granite.

Nevertheless, irrespective of the origin of the discrepancy between these ages, the age of 294 ± 1 Ma found for the syntectonic Montalet granite confirms the existence of a major magmatic event that accompanies crustal extension during the Late Palaeozoic in the southern French MC (Van Den Driessche and Brun, 1989).

The cause and the modes of the extension that is supposed to be responsible for the decay of the Variscan belt are still debated, but all studies agree that the period between 330 Ma and 290 Ma is a critical one: it corresponds to the vanishing of plate convergence and the onset of crustal extension (e.g. Burg et al., 1994). The present study emphasizes the absolute need for precise dating to refine this evolution and decipher the possible causal relation between these two major tectonic processes.

References

Beaud, F., 1985. Étude structurale de la zone axiale de la Montagne Noire (sud du Massif Central français). Détermination des mécanismes de déformation, relation avec les nappes du versant sud. Ph.D. thesis, Université des sciences et techniques du Languedoc, 191 p.

Bé Mézème, E., 2005. Contribution de la géochronologie U-Th-Pb sur monazite à la compréhension de la fusion crustale dans la chaîne hercynienne française et implication géodynamique. Ph.D. thesis, Université d'Orléans, 277 p.

Berthé, D., Choukroune, P., Jegouzo, P., 1979. Orthogneiss, mylonites and non-coaxial deformation of granites: the example of the South Armorican Shear Zone. J. Struct. Geol. 11, 31–42.

Bruguier, O., Becq-Giraudon, J.F., Champenois, M., Deloule, E., Ludden, J., Mangin, D., 2003. Application of in situ zircon geochronology and accessory phase chemistry to constraining basin development during post-collisional extension: a case study from the French Massif Central. Chem. Geol. 201, 319–336.

Brun, J.P., Van Den Driessche, J., 1994. Extensional gneiss domes and detachment fault systems: structure and kinematics. Bull. Soc. geol. France 165, 519–530.

Brun, J.P., Van Den Driessche, J., 1996. Réponse aux observations et remarques sur l'article « Extensional gneiss domes and detachment fault systems: structure and kinematics » (Demange M., Bull. Soc. geol. France 167, 295–298). Bull. Soc. geol. France 167, 298–302.

Burg, J.P., Van Den Driessche, J., Brun, J.P., 1994. Syn- to post-thickening extension: mode and consequences. C. R. Acad. Sci. Paris, Ser. II 319, 1019–1032.

Charles, N., Faure, M., Chen, Y., 2009. The Montagne Noire migmatitic dome emplacement (French Massif Central): new insights from petro-fabric and AMS studies. J. Struct. Geol. 31, 1423–1440.

Demange, M., 1996. Observations et remarques sur l'article « Extensional gneiss domes and detachment fault systems: structure and kinematics » (Brun J.P. and Van Den Driessche J., Bull. Soc. geol. France 165, 519–530). Bull. Soc. Geol. France 167, 295–298.

Demange, M., Guérangé-Lozes, J., Guérangé, B., et al., 1995. Notice explicative, Carte géol. France (1/50,000), feuille Lacaune (987). Orléans: BRGM, 153 p. Geological map by M. Demage, J. Guérangé-Lozes, B. Guérangé. 1995.

Echtler, H., Malavieille, J., 1990. Extensional tectonics, basement uplift and Stephano-Permian collapse basin in a Late Variscan metamorphic core complex (Montagne Noire, southern Massif Central). Tectonophysics 177, 125–138.

Faure, M., Cocherie, A., Bé Mézème, E., Charles, N., Rossi, P., 2010. Middle Carboniferous crustal melting in the Variscan Belt: new insights from U-Th-Pbtot. monazite and U-Pb zircon ages of the Montagne Noire Axial Zone (southern French Massif Central). Gondwana Research 18, 653–673.

Gapais, D., Barbarin, B., 1986. Quartz fabric transition in a cooling syntectonic granite (Hermitage massif, France). Tectonophysics 125, 357–370.

Gasquet, D., Bertrand, J.M., Paquette, J.L., Lehmann, J., Ratzov, G., De Ascenção Guedes, R., Tiepolo, M., Boullier, A.M., Scaillet, S., Nomade, S., 2010. Miocene to Messinian deformation and hydrothermalism in the Lauzière Massif (French Western Alps): new U-Th-Pb and Argon ages. Bull. Soc. geol. France 181, 227–241.

Hurai, V., Paquette, J.L., Huraiová, M., Konečný, P., 2010. U-Th-Pb geochronology of zircon and monazite from syenite and pincinite xenoliths in Pliocene alkali basalts of the intra-Carpathian back-arc basin. J. Volcanol. Geotherm. Res. 198, 275–287.

Jackson, S.E., Pearson, N.J., Griffin, W.L., Belousova, E.A., 2004. The application of laser ablation inductively coupled plasma mass spectrometry to in situ U-Pb zircon geochronology. Chem. Geol. 211, 47–69.

Ludwig, K.R., 1998. On the treatment of concordant uranium-lead ages. Geochim. Cosmochim. Acta 62, 665–676.

Ludwig, K.R., 2001. User's manual for Isoplot/Ex Version 2.49, a geochronological toolkit for Microsoft Excel. Spec Publ., 1a. Berkeley Geochronological Center, Berkeley, USA.

Maluski, H., Costa, S., Echtler, H., 1991. Late Variscan tectonic evolution by thinning of earlier thickened crust. An ^{40}Ar-^{39}Ar study of the Montagne Noire, southern Massif Central, France. Lithos 26, 287–304.

Paquette, J.L., Tiepolo, M., 2007. High resolution (5 μm) U-Th-Pb isotopes dating of monazite with excimer laser ablation (ELA)-ICPMS. Chem. Geol. 240, 222–237.

Pitra, P., Ballèvre, M., Ruffet, G., 2010. Inverted metamorphic field gradient towards a Variscan suture zone (Champtoceaux Complex, Armorican Massif, France). J. Metam. Geol. 28, 183–208.

Simpson, C., Wintsch, R.P., 1989. Evidence for deformation-induced K-feldspar replacement by myrmekite. J. Metam. Geol. 7, 261–275.

Van Den Driessche, J., Brun, J.P., 1989. Un modèle cinématique de l'extension Paléozoïque supérieur dans le sud du Massif central. C. R. Acad. Sci, Paris, Ser. II 309, 1607–1613.

Van Den Driessche, J., Brun, J.P., 1992. Tectonic evolution of the Montagne Noire (French Massif Central): a model of extensional gneiss dome. Geodinamica Acta 5, 85–99.

Wiedenbeck, M., Allé, P., Corfu, F., Griffin, W.L., Meier, M., Oberli, F., von Quadt, A., Roddick, J.C., Spiegel, W., 1995. Three natural zircon standards for U-Th-Pb, Lu-Hf, trace element and REE analyses. Geostand. Newslett. 19, 1–23.